Editors' Suggestion

Transition between Heavy-Fermion-Strange-Metal and Quantum Spin Liquid in a 4d-Electron Trimer Lattice

Hengdi Zhao[1], Yu Zhang[1], Pedro Schlottmann[2], Rahul Nandkishore,[1,3] Lance E. DeLong[4], and Gang Cao[1,5,*]

[1]*Department of Physics, University of Colorado at Boulder, Boulder, Colorado 80309, USA*
[2]*Department of Physics, Florida State University, Tallahassee, Florida 32306, USA*
[3]*Center for Theory of Quantum Matter, University of Colorado at Boulder, Boulder, Colorado 80309, USA*
[4]*Department of Physics and Astronomy, University of Kentucky, Lexington, Kentucky 40506, USA*
[5]*Center for Experiments on Quantum Materials, University of Colorado at Boulder, Boulder, Colorado 80309, USA*

We present experimental evidence that a heavy Fermi surface consisting of itinerant, charge-neutral spinons underpins both heavy-fermion-strange-metal (without f electrons) and quantum-spin-liquid states in the 4d-electron trimer lattice, $Ba_4Nb_{1-x}Ru_{3+x}O_{12}(|x| < 0.20)$. These two exotic states both exhibit an extraordinarily large entropy, a linear heat capacity extending into the milli-Kelvin regime, a linear thermal conductivity at low temperatures, and separation of charges and spins. Furthermore, the insulating spin liquid is a much better thermal conductor than the heavy-fermion-strange-metal that separately is observed to strongly violate the Wiedemann-Franz law. We propose that at the heart of this 4d system is a universal, heavy spinon Fermi surface that provides a unified framework for explaining the exotic phenomena observed throughout the entire series. The control of such exotic ground states provided by variable Nb concentration offers a new paradigm for studies of correlated quantum matter.

Planckian strange metals [1–15], heavy-fermion metals [16–26], and quantum spin liquids [27–34] are intriguing quantum states of matter currently subject to intense investigation. Planckian metals feature a linear temperature T dependence of electrical resistivity ρ that persists to $T = 0$ K, independent of the Fermi surface topology, because charge carriers scatter at a rate that saturates in the Planckian limit, $1/\tau = \alpha k_B T/\hbar$ (where τ is the relaxation time, k_B and $\hbar$ the Boltzmann and reduced Planck's constants, respectively, and α a constant of order unity [2–11]).

Heavy-fermion metals, on the other hand, are characterized by a large Sommerfeld coefficient γ arising from electronic contributions to low-T heat capacity $C(T)$. Values of γ range from 20 mJ/mol K² [17] to up to 1600 mJ/mol K² [19]. At the present time, the heavy-fermion behavior is observed almost exclusively in 4f- and 5f-electron materials and is dictated by hybridization between itinerant and localized magnetic electron states [21–25]. A notable exception to the ongoing predominance of heavy f-electron states is the transition metal oxide LiV_2O_4. This material exhibits a very high $\gamma = 420$ mJ/mol K² [35–37] and $\rho \propto T^2$ in the low-T limit [37]. The heavy-fermion behavior is thought to be a consequence of its frustrated lattice [38–40]. Heavy-fermion fractionalization driven by an interplay between geometric frustration and the Kondo effect also has been extensively discussed in recent years in part because the one-dimensional Doniach "Kondo necklace" scenario [41] may not be flexible enough to account for non-Fermi liquid behavior in heavy-fermion systems; see, e.g., [18,21,25,26].

Finally, quantum spin liquids are among the most intensively studied states of condensed matter. Theoretical treatments of the honeycomb iridates, α-RuCl₃, and other triangular lattices have inspired a large body of experimental work that seeks to identify various types of quantum spin liquids whose experimental signatures include a linear $C(T)$ extending to $T = 0$ K, which is expected to arise from a Fermi surface of charge-neutral spinons [27–34,42].

Each of the three states mentioned above typically occurs in different classes of materials with distinct energy scales. In contrast, we have synthesized the single-crystal series $Ba_4Nb_{1-x}Ru_{3+x}O_{12}(|x| < 0.20)$ [Figs. 1(a)–1(c)] that, depending on composition x, exhibits the characteristics of all three exotic states, as well as completely novel phenomena. At one end of the series, a novel metal simultaneously exhibits the characteristics of both a strange metal [α is of order unity; see Fig. 1(d)] and a heavy-fermion metal [$\gamma = 164$ mJ/mol K²; see Fig. 1(e)]. Furthermore, this metal violates the Wiedemann-Franz (WF) law by up to a factor of 26 [Fig. 1(f)] and exhibits a sign change in the Hall effect when the current is applied along different crystalline directions (Fig. S6 in Supplemental Material [43]). We term this material a heavy-fermion-strange-metal. At the other end of the series, a strongly frustrated Mott insulator exhibits an increased $\gamma = 225$ mJ/mol K² and an
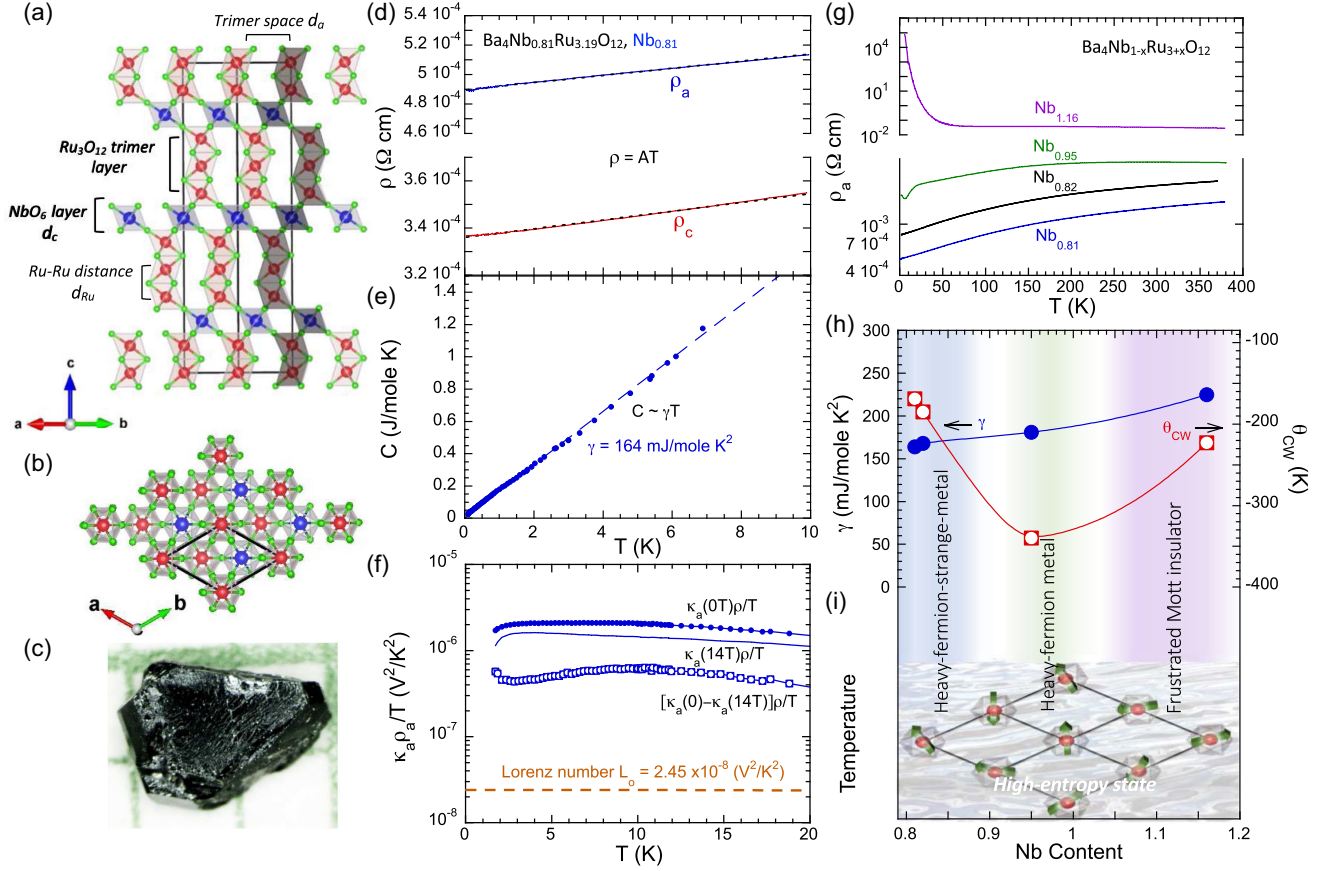
FIG. 1. Key features and phase diagram. (a) The crystal structure of $Ba_4Nb_{1-x}Ru_{3+x}O_{12}$ along the c axis, and (b) the ab plane. (c) A single crystal of $Nb_{0.81}$. The T dependence for 50 mK $< T <$ 10 K for $Nb_{0.81}$ of (d) the a-axis ρ_a and the c-axis ρ_c (black dashed lines are linear fit), and (e) $C(T)$. (f) The Lorenz number of the WF law $L_o = \kappa/\sigma T$ and the measured $\kappa_a \rho_a/T$ for $1.8 < T < 20$ K for $Nb_{0.81}$. (g) The T dependence of ρ_a for 50 mK $< T <$ 380 K for $Nb_{0.81}$, $Nb_{0.82}$, $Nb_{0.95}$, and $Nb_{1.16}$. (h) γ (blue) and θ_{CW} (red, right scale) as a function of the Nb content. (i) A schematic phase diagram.

enhanced thermal conductivity κ greater than that of the metal. A heavy-fermion metal with $\gamma = 181$ mJ/mol K^2 is situated between these two end states [Fig. 1(h)]. The electrical resistivity ρ progressively changes with Nb content [Fig. 1(g)], but a strikingly linear $C(T)$ extending down to 50 mK, an equally linear low-T κ, and a paramagnetic state with a strong exchange energy of up to 340 K persist throughout the entire series [Figs. 1(h) and 1(i)]. A large entropy with no discernible long-range order extends into the milli-Kelvin regime for all Nb compositions studied [Fig. 1(h)].

The larger κ of the insulating state compared to that of the metallic state forcefully argues that a heavy Fermi surface of itinerant charge-neutral spinons must be invoked to explain this behavior throughout the series [Figs. 1(h) and 1(i)]. Importantly, it rules out the possibility that the large linear-T $C(T)$ in the insulator comes from localized degrees of freedom that could not contribute to κ. We stress that this scenario explains a large array of exotic phenomena in terms of a dissociation of charges and spins, as discussed below. This rich, novel phenomenology arises from a rare interplay

between geometric frustration and competing interactions and provides a compelling new paradigm for correlated quantum materials. Note that polycrystalline $Ba_4NbRu_3O_{12}(x = 0)$ has been reported to be a geometrically frustrated insulator with $\gamma = 31$ mJ/mol K^2 with spin freezing near 4 K [44], which is not discerned in this study.

Our single-crystal x-ray diffraction data gathered between 100 K and 300 K indicate that the series of $Ba_4Nb_{1-x}Ru_{3+x}O_{12}$ (for $|x| < 0.20$; the sign of x can be either positive or negative) adopts a rhombohedral structure with the space group R-3 (No. 148), which is retained for all x studied herein (Fig. S1 and Tables S1–S3 in Supplemental Material [43]). For simplicity, we use $Nb_{0.81}$, $Nb_{0.95}$, $Nb_{1.00}$, and $Nb_{1.16}$ to denote $Ba_4Nb_{1-x}Ru_{3+x}O_{12}$ with different x values. The crystal structural data indicate that the formal valence of Nb is 5+ ($4d^0$) across the entire series [44]. The average valence of Ru decreases with increasing Nb content from 3.75+ for $Nb_{0.81}$ to 3.69+ for $Nb_{0.95}$ and to 3.59+ for $Nb_{1.16}$, indicating a mixed valence of $Ru^{3+}(4d^5)$ and $Ru^{4+}(4d^4)$, which is common among perovskite ruthenates [45]. The average number of $4d$ electrons in each Ru_3O_{12}
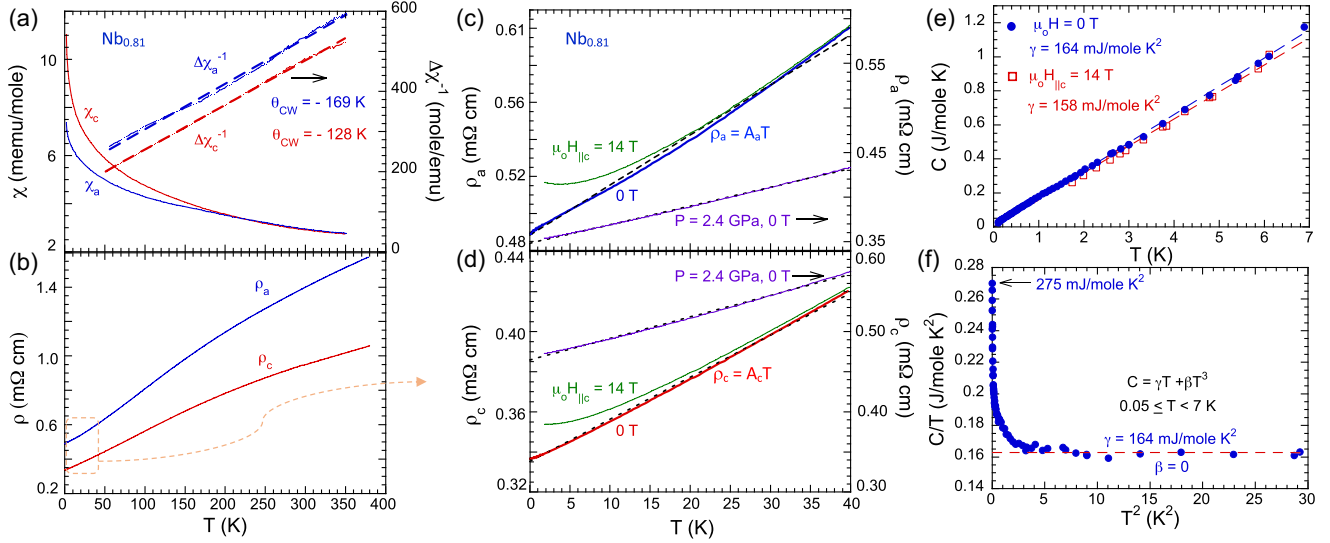
FIG. 2.   Physical properties of $Nb_{0.81}$. The T dependence of (a), the a-axis and c-axis χ_a and χ_c along with $\Delta\chi_a^{-1}$ and $\Delta\chi_c^{-1}$ (right scale), and (b) ρ_a and ρ_c for 50 mK $< T <$ 380 K. (c), (d) ρ_a and ρ_c for 50 mK $< T <$ 40 K at $\mu_o H_{||c} = 0$ and 14 T, and at $P = 2.4$ GPa and $H = 0$ (right scale) (black dashed lines are linear fit). (e) The T dependence of $C(T)$ at $\mu_o H_{||c} = 0$ and 14 T. (f) $C(T)$ vs T^2.

trimer is estimated to be 12.75, 12.93, 13, and 13.23 in $Nb_{0.81}$, $Nb_{0.95}$, $Nb_{1.00}$, and $Nb_{1.16}$, respectively.

The key structural element of $Ba_4Nb_{1-x}Ru_{3+x}O_{12}$ is the Ru_3O_{12} trimer formed by three face-sharing RuO_6 octahedra. The trimers (red) are linked along the c axis [Fig. 1(a)] by corner-sharing NbO_6 octahedra (blue) to form the triangular ab planes or trimer layers, which is a common source of geometric frustration [Figs. 1(b) and 1(i)] [43].

We discuss below the definitive characteristics of each of the three exotic states shown in Fig. 1(i). Additional data are included in the Supplemental Material [43].

Heavy-fermion-strange-metal.—The magnetic susceptibility χ of $Nb_{0.81}$ exhibits a robust Curie-Weiss behavior down to 1.7 K [Fig. 2(a)]. An analysis of the data for 50–350 K yields the Curie-Weiss temperature $\theta_{CW} = -169$ K and -128 K for the a-axis χ_a and c-axis χ_c, respectively, which reflects a strong antiferromagnetic coupling. The paramagnetic susceptibility is on the order 10^{-3} emu/mol, comparable to the values observed for heavy-fermion systems [19] (see Table S4 in Supplemental Material [43]).

The resistivities ρ of $Nb_{0.81}$ from 50 mK to 380 K for current along the a-axis ρ_a and c-axis ρ_c are shown in Figs. 2(b)–2(d) (note that $\rho_a > \rho_c$). The linearity in T in both ρ_a and ρ_c for T > 250 K is a common occurrence in many correlated oxides due to enhanced electron-electron and electron-phonon interactions [15]. What is intriguing is that the linearity in both $\rho_a(= A_aT)$ and $\rho_c(= A_cT)$ persists from 50 K down to 50 mK [Figs. 1(d), 2(c), and 2(d)], with slope values $A_a = 2.45 \times 10^{-6}$ Ω cm/K and $A_c = 1.88 \times 10^{-6}$ Ω cm/K. Our estimate of the Planckian limit yields lower bounds for $\alpha = 0.46$ and 0.75 for the a axis and c axis, respectively [43], confirming that the scattering rate of charge carriers in $Nb_{0.81}$ is indeed

close to the Planckian limit (Fig. S2a in Supplemental Material [43]). Note that the Hall coefficient changes sign with current orientation, indicating that the Fermi surface of the metallic $Nb_{0.81}$ is highly anisotropic (Fig. S6 in Supplemental Material [43]).

The linearity of ρ_a and ρ_c persists in the presence of applied pressure P up to 2.4 GPa [right scale in Figs. 2(c) and 2(d)], reflecting that the scattering rate is insensitive to any possible changes in the crystal and/or electronic structures due to applied pressure. However, application of magnetic field H changes scattering processes, resulting instead in a nearly T^2-dependence for both ρ_a and ρ_c at low T, as expected for a Fermi liquid [Figs. 2(c) and 2(d), and Supplemental Material Fig. S2b [43]].

As for the low-T heat capacity $C(T)$ at 14 T [Fig. 2(e)], the slope of the linear T dependence of $C(T)$ changes only slightly from $\gamma = 164$ mJ/mol K^2 at $\mu_o H = 0$ to $\gamma = 158$ mJ/mol K^2 at $\mu_o H = 14$ T [Fig. 2(e)]. It is particularly striking that the high γ value persists in such a strong field that normally depresses entropy, but this behavior is consistent with $C(T)$ being dominated by a spinon Fermi surface [27,28,34,42,46].

It is curious that the T^3 contribution to $C(T)$ below 7 K [parametrized by the second term in $C(T) = \gamma T + \beta T^3$] is essentially zero [Fig. 2(f)]. The phonon contribution (positive β) is compensated by the second term of the Sommerfeld expansion of the electronic contribution (negative β) yielding a measured β that is essentially zero. The low-T $C(T)$ is then γT [Fig. 2(f)] [43]. Note that $\gamma(= C/T)$ rapidly rises to 275 mJ/mol K^2 at 50 mK. The nearly 70% increase in γ is intriguing since γ is not expected to be a strong function of T in the low-T limit in the absence of magnetic order, but it hints at a low-energy scale ~3 K.
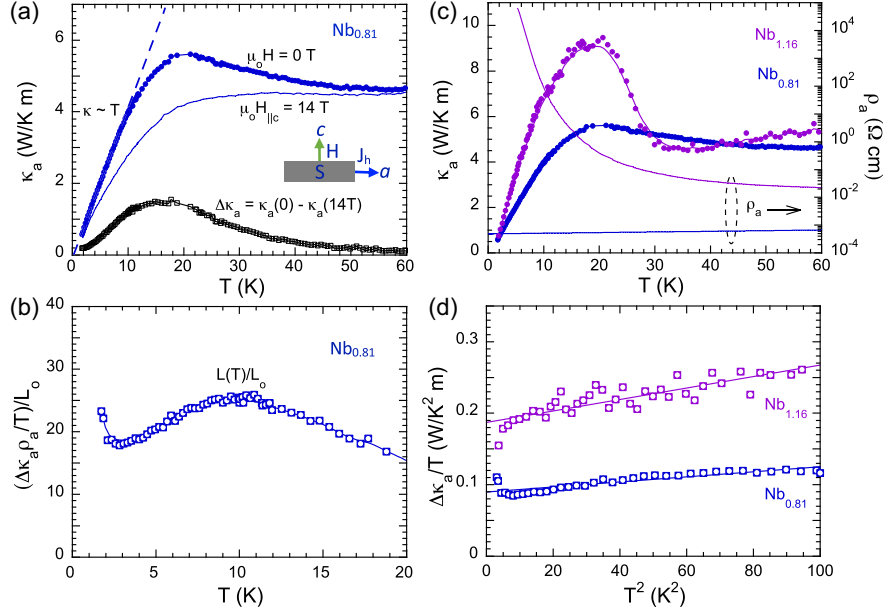
FIG. 3. Thermal conductivity of $Nb_{0.81}$ and $Nb_{1.16}$. The T dependence of (a) $\kappa_a(0)$ at $H = 0$, $\kappa_a(14T)$ and $\Delta\kappa_a = \kappa_a(0) - \kappa_a(14T)$ below 60 K, and (b) $L(T)/L_o$ where $L_o = 2.45 \times 10^{-8}$ (V^2/K^2) and the measured $L(T) = \Delta\kappa_a\rho_a/T$. Inset: the configuration for κ_a measurements; J_h is thermal current density. (c) The T dependence of κ_a and ρ_a (right scale) for $Nb_{0.81}$ and $Nb_{1.16}$. Note the inverse relationship between κ_a and ρ_a for $Nb_{1.16}$. (d) $\Delta\kappa_a/T$ vs T^2 for metallic $Nb_{0.81}$ and insulating $Nb_{1.16}$. Note the intercept of $\Delta\kappa_a/T$ at $T = 0$ K is larger for $Nb_{1.16}$ than for $Nb_{0.81}$.

Note that this upturn in C/T is supplanted by a downturn in $Nb_{1.16}$, as discussed below, which helps rule out a nuclear Schottky anomaly with a signature term in $C(T) \sim 1/T^2$ (Fig. S3b in Supplemental Material [43]); this is also confirmed by our heat capacity data on $BaRuO_3$ and Nb_2O_5 measured in 50 mK–1.0 K and at $\mu_oH = 0$ and 14T, which do not follow at all $C(T) \sim 1/T^2$, indicating a clear absence of any discernible nuclear Schottky contributions to $C(T)$ of $Nb_{0.81}$ [43,47].

The thermal conductivity $\kappa_a(0)$ of $Nb_{0.81}$ along the a axis also decreases linearly with decreasing T below 10 K [Fig. 3(a)]. At $\mu_oH_{\parallel c} = 14$ T, κ_a responds strongly to H for $2 < T < 60$ K, but very weakly beyond this range. The difference $\kappa_a(0) - \kappa_a(14T)$ yields $\Delta\kappa_a$ that reflects contributions from heat carriers that are susceptible to magnetic fields [Fig. 3(a)] [43]. The same is true for κ_c (see Fig. S4 of Supplemental Material [43]).

Thermal and electrical currents are normally carried by the same quasiparticles. This is reflected in the WF law $\kappa/\sigma = L_oT$, which states that for a single band the ratio of κ to electrical conductivity σ is proportional to T with a constant of proportionality = Lorenz number L_o. Here, using $\Delta\kappa_a$, $L(T) = \Delta\kappa_a\rho_a/T(\sigma \cong 1/\rho)$ we obtain $L > L_o$ by a factor of up to 26 [see squares in Figs. 3(b) and 1(f)]. Such a strong violation of the WF law suggests that the relaxation times are vastly different for thermal and electrical processes or that more than one band is participating.

The WF law works well for typical metals, including Fermi liquids [48] when the condition of elastic scattering

is satisfied [49]. Inelastic processes result in different relaxation times for charge and heat transport [43]. The strong violation of the WF law is likely due to a combined effect of geometric frustration and low dimensionality that causes a dissociation of charges and spins [45,46,50–56], whose presence is reinforced by the inverse relationship between κ_a and σ_a. The electrical insulator $Nb_{1.16}$, whose ρ_a is 10^7 greater than that for the metal $Nb_{0.81}$ at low T, is a much better thermal conductor than the metal $Nb_{0.81}$ below 30 K [Fig. 3(c)]. This is clearer in Fig. 3(d) in which the intercept of $\Delta\kappa_a/T$ at $T = 0$ for the insulating $Nb_{1.16}$ is nearly twice as large as that for the metallic $Nb_{0.81}$. Note the linearity of $\kappa_a(0)$ for both $Nb_{0.81}$ and $Nb_{1.16}$ below 10 K [Fig. 3(c)].

Heavy-fermion metal and frustrated insulator.—Increasing the Nb content in $Ba_4Nb_{1-x}Ru_{3+x}O_{12}$ weakens the metallic state and eventually induces the insulating state. The weakened metallic state in $Nb_{0.95}$ and the insulating state in $Nb_{1.16}$ retain paramagnetic spin correlations [Figs. 4(a) and 4(b)] with a strong exchange energy (absolute values of θ_{CW}) up to 340 K and enhanced γ values [Fig. 1(h)]. In $Nb_{0.95}$, both ρ_a and ρ_c decrease below 150 K [Fig. 4(c)]. The insulator $Nb_{1.16}$ displays a drastic increase in ρ by more than 7 orders of magnitude with decreasing T [Fig. 4(d)]. However, this electrical insulator $Nb_{1.16}$ is a much better thermal conductor than the metal $Nb_{0.81}$ [Figs. 3(c) and 3(d)]. This contrasting behavior further implicates the dissociation of charges and spins and itinerant spinons (more data and discussion on κ
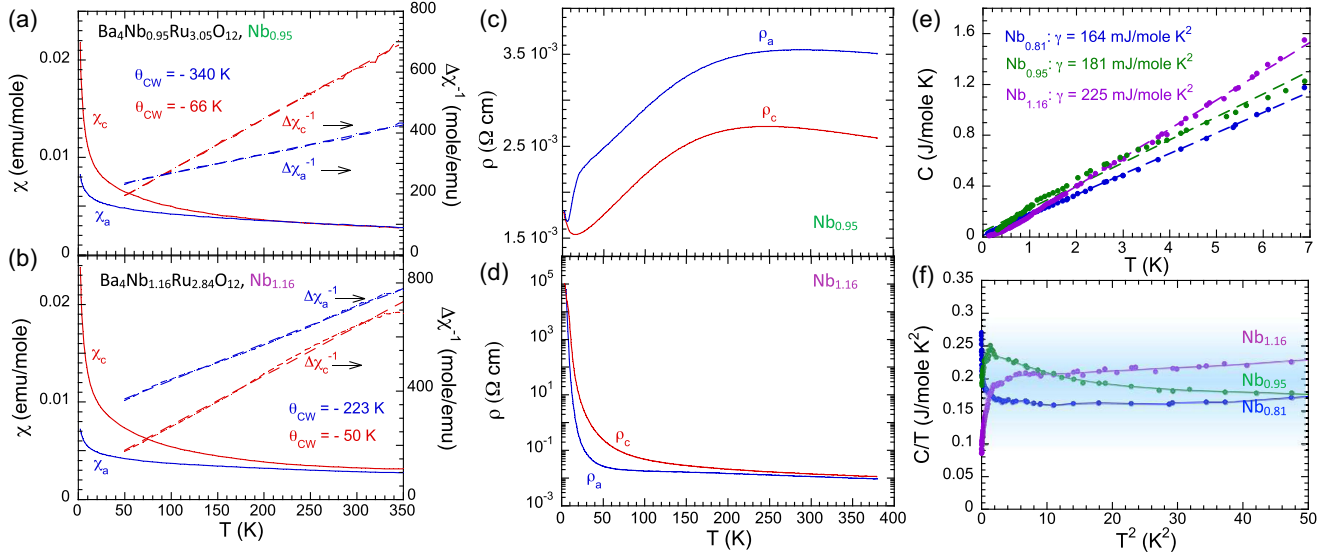
FIG. 4. Physical properties of $Nb_{0.95}$ and $Nb_{1.16}$. The T dependence of χ_a and χ_c along with $\Delta\chi_a^{-1}$ and $\Delta\chi_c^{-1}$ (right scale) for (a) $Nb_{0.95}$ and (b) $Nb_{1.16}$. The T dependence of ρ_a and ρ_c for (c) $Nb_{0.95}$ and (d) $Nb_{1.16}$. (e) $C(T)$ for 50 mK $< T <$ 7 K and (f) C/T vs T^2 for $Nb_{0.95}$, $Nb_{1.16}$, and $Nb_{0.81}$.

at magnetic fields are presented in Fig. S7 of the Supplemental Material [43]).

$C(T)$ of both $Nb_{0.95}$ and $Nb_{1.16}$ remains essentially linear (with slight deviations) below 0.5 K and yields even larger values of $\gamma = 181$ and 225 mJ/mol K^2 for $Nb_{0.95}$ and $Nb_{1.16}$, respectively [Fig. 4(e)]. The linearity of $C(T)$ in both $Nb_{0.95}$ and $Nb_{1.16}$ also remains unchanged at 14 T and higher temperatures, ruling out the influences of magnetic impurities and further emphasizing the persistent Fermi surface of charge-neutral spinons (Fig. S5 in Supplemental Material [43]). Note that the linearity of $C(T)$ in the insulating phase cannot be due to localized excitations since such excitations would not contribute to κ. The abrupt upturn in C/T vs T^2 below 0.5 K in $Nb_{0.81}$ is replaced by an equally abrupt downturn in $Nb_{1.16}$ [Fig. 4(f)] [43].

The most striking feature shared by the entire $Ba_4Nb_{1-x}Ru_{3+x}O_{12}$ series is the persistent linearity in low-T $C(T)$ and κ, and extraordinarily large γ, independent of the ground state type [Figs. 3(a), 3(c), 4(e), and 4(f)]. All of our results constitute compelling evidence for the existence of a heavy-fermion-strange-metal [Figs. 1(d) and 1(e)] [43] and a quantum spin liquid [Figs. 3(c), 3(d), and 4(d)–4(f)] depending on the Nb content. The complex behavior of $Ba_4Nb_{1-x}Ru_{3+x}O_{12}$ suggests a powerful simplifying principle: At the heart of this 4d system is a universal, itinerant, heavy spinon Fermi surface that provides a unified framework for explaining the exotic phenomena observed throughout the entire series: (1) the large exchange energy (θ_{CW}) but no magnetic order [Figs. 1(h)], (2) the linear $C(T)$ persistent down to 50 mK, indicating a nonzero low-energy density of states [Figs. 2(e) and 4(e)], (3) the extraordinarily large γ only seen in heavy-fermion

materials [Figs. 1(h) and 4(e)], and (4) the linear κ at low T in all states, and much larger κ in the insulating spin liquid than in the heavy-fermion-strange-metal [Figs. 3(c) and 3(d)], which separately is observed to strongly violate the Wiedemann-Franz law [Figs. 1(d)–1(f)].

In summary, $Ba_4Nb_{1-x}Ru_{3+x}O_{12}$ is a rare system, if not the first, to encompass a proximity or even coexistence of both spin liquid physics, strong electron correlations tunable across a Mott metal-to-insulator transition, and a heavy-fermion-strange-metal. Clearly, the rich, exotic phenomenology offers a compelling new paradigm of correlated quantum matter.

*Corresponding author: gang.cao@colorado.edu

[1] H. Takagi, B. Batlogg, H. L. Kao, J. Kwo, R. J. Cava, J. J. Krajewski, and W. F. Peck, Jr., Systematic evolution of temperature-dependent resistivity in La$_{2-x}$Sr$_x$CuO$_4$, Phys. Rev. Lett. **69**, 2975 (1992).

[2] O. Parcollet and A. Georges, Non-Fermi-liquid regime of a doped Mott insulator, Phys. Rev. B **59**, 5341 (1999).

[3] J. Zaanen, Why the temperature is high, Nature (London) **430**, 512 (2004).

[4] R. A. Cooper et al., Anomalous criticality in the electrical resistivity of La$_{2-x}$Sr$_x$CuO$_4$, Science **323**, 603 (2009).

[5] L. Taillefer, Scattering and pairing in cuprate superconductors, Annu. Rev. Condens. Matter Phys. **1,** 51 (2010).

[6] J. A. N. Bruin, H. Sakai, R. S. Perry, and A. P. Mackenzie, Similarity of scattering rates in metals showing T-linear resistivity, Science **339,** 804 (2013).

[7] Peter Cha, Nils Wentzell, Olivier Parcollet, Antoine Georges, and Eun-Ah Kim, Linear resistivity, and Sachdev-Ye-Kitaev (SYK) spin liquid behavior in a quantum critical metal with spin-1/2 fermions, Proc. Natl. Acad. Sci. U.S.A. **117,** 18341 (2020).

[8] Haoyu Guo, Yingfei Gu, and Subir Sachdev, Linear in temperature resistivity in the limit of zero temperature from the time reparameterization soft mode, Ann. Phys. (Amsterdam) **418,** 168202 (2020).

[9] G. Grissonnanche, Y. Fang, A. Legros, S. Verret, F. Laliberté, C. Collignon, J. Zhou, D. Graf, P. A. Goddard, L. Taillefer, and B. J. Ramshaw, Linear-in temperature resistivity from anisotropic Planckian scattering rate, Nature (London) **595,** 667 (2021).

[10] A. Legros, S. Benhabib, W. Tabis, F. Laliberté, M. Dion, M. Lizaire, B. Vignolle, D. Vignolles, H. Raffy, Z. Z. Li, P. Auban-Senzier, N. Doiron-Leyraud, P. Fournier, D. Colson, L. Taillefer, and C. Proust, Universal T-linear resistivity and Planckian dissipation in overdoped cuprates, Nat. Phys. **15,** 142 (2019).

[11] C. Yang, H. Liu, Y. Liu, J. Wang, D. Qiu, S. Wang, Y. Wang, Q. He, X. Li, P. Li, Y. Tang, J. Wang, X. C. Xie, J. M. Valles, Jr., J. Xiong, and Y. Li, Signatures of a strange metal in a bosonic system, Nature (London) **601,** 205 (2022).

[12] Y. Cao, D. Chowdhury, D. Rodan-Legrain, O. Rubies-Bigorda, K. Watanabe, T. Taniguchi, T. Senthil, and P. Jarillo-Herrero, Strange metal in magic-angle graphene with near Planckian dissipation, Phys. Rev. Lett. **124,** 076801 (2020).

[13] I. M. Hayes, N. Maksimovic, G. N. Lopez, M. K. Chan, B. J. Ramshaw, R. D. McDonald, and J. G. Analytis, Superconductivity and quantum criticality linked by the Hall effect in a strange metal, Nat. Phys. **17,** 58 (2021).

[14] Y. Nakajima, T. Metz, and C. Eckberg, Quantum-critical scale invariance in a transition metal alloy, Commun. Phys. **3,** 181 (2020).

[15] P. T. Brown, D. Mitra, E. Guardado-Sanchez, R. Nourafkan, A. Reymbaut, C.-D. Hébert, S. Bergeron, A.-M. S. Tremblay, J. Kokalj, D. A. Huse, P. Schauss, and W. S. Bakr, Bad metallic transport in a cold atom Fermi-Hubbard system, Science **363,** 379 (2019).

[16] F. Steglich, J. Aarts, C. D. Bredl, W. Lieke, D. Meschede, W. Franz, and H. Schafer, Superconductivity in the presence of strong Pauli paramagnetism: $CeCu_2Si_2$, Phys. Rev. Lett. **43,** 1892 (1979).

[17] L. E. DeLong, J. G. Huber, K. N. Yang, and M. B. Maple, Observation of high-field superconductivity of a strongly interacting Fermi liquid in U_6Fe, Phys. Rev. Lett. **51,** 312 (1983).

[18] T. Senthil, M. Vojta, and S. Sachdev, Weak magnetism and non-Fermi liquids near heavy-fermion critical points, Phys. Rev. B **69,** 035111 (2004).

[19] G. R. Stewart, Heavy-fermion systems, Rev. Mod. Phys. **56,** 755 (1984).

[20] H. v. Löhneysen, T. Pietrus, G. Portisch, H. G. Schlager, A. Schröder, M. Sieck, and T. Trappmann, Non-Fermi-liquid behavior in a heavy-fermion alloy at a magnetic instability, Phys. Rev. Lett. **72,** 3262 (1994).

[21] H. v. Löhneysen, A. Rosch, M. Vojta, and P. Wölfle, Fermi-liquid instabilities at magnetic quantum phase transitions, Rev. Mod. Phys. **79,** 1015 (2007).

[22] Qimiao Si and Frank Steglich, Heavy fermions, and quantum phase transitions, Science **329,** 1161 (2010).

[23] Pedro Schlottmann, Non-Fermi liquid behavior in heavy fermion systems, in *Handbook of Magnetic Materials*, edited by K. H. J. Buschow (Elsevier, Amsterdam, 2015), Vol. 23, Chap. 2, pp. 85–160.

[24] B. D. White, J. D. Thompson, and M. B. Maple, Unconventional superconductivity in heavy-fermion compounds, Physica (Amsterdam) **514C,** 246 (2015).

[25] P. Coleman and A. H. Nevidomskyy, Frustration and the Kondo effect in heavy fermion materials, J. Low Temp. Phys. **161,** 182 (2010).

[26] S. Paschen and Q. Si, Quantum phases driven by strong correlations, Nat. Rev. Phys. **3,** 9 (2021).

[27] P. W. Anderson, The resonating valence bond state in La_2CuO_4 and superconductivity, Science **235,** 1196 (1987).

[28] P. A. Lee, An end to the drought of quantum spin liquids, Science **321,** 1306 (2008).

[29] L. Savary and L. Balents, Quantum spin liquids: A review, Rep. Prog. Phys. **80,** 016502 (2017).

[30] Y. Zhou, K. Kanoda, and T.-K. Ng, Quantum spin liquid states, Rev. Mod. Phys. **89,** 025003 (2017).

[31] C. Broholm, R. Cava, S. Kivelson, D. Nocera, M. Norman, and T. Senthil, Quantum spin liquids, Science **367,** 263 (2020).

[32] B. Lake, D. A. Tennant, C. D. Frost, and S. E. Nagler, Quantum criticality and universal scaling of a quantum antiferromagnet, Nat. Mater. **4,** 329 (2005).

[33] M. Mourigal, M. Enderle, A. Klöpperpieper, J.-S. Caux, A. Stunault, and H. M. Rønnow, Fractional spinon excitations in the quantum Heisenberg antiferromagnetic chain, Nat. Phys. **9,** 435 (2013).

[34] S. Yamashita, Y. Nakazawa, M. Oguni, Y. Oshima, H. Nojiri, Y. Shimizu, K. Miyagawa, and K. Kanoda, Thermodynamic properties of a spin-1/2 spin-liquid state in a κ-type organic salt, Nat. Phys. **4,** 459 (2008).

[35] S. Kondo, D. C. Johnston, C. A. Swenson, F. Borsa, A. V. Mahajan, L. L. Miller, T. Gu, A. I. Goldman, M. B. Maple, D. A. Gajewski, E. J. Freeman, N. R. Dilley, R. P. Dickey, J. Merrin, K. Kojima, G. M. Luke, Y. J. Uemura, O. Chmaissem, and J. D. Jorgensen, LiV_2O_4: A heavy fermion transition metal oxide, Phys. Rev. Lett. **78,** 3729 (1997).

[36] O. Chmaissem, J. D. Jorgensen, S. Kondo, and D. C. Johnston, Structure and thermal expansion of LiV_2O_4: Correlation between structure and heavy fermion behavior, Phys. Rev. Lett. **79,** 4866 (1997).

[37] C. Urano, M. Nohara, S. Kondo, F. Sakai, H. Takagi, T. Shiraki, and T. Okubo, LiV_2O_4 spinel as a heavy-mass Fermi liquid: Anomalous transport and role of geometrical frustration, Phys. Rev. Lett. **85,** 1052 (2000).

[38] V. I. Anisimov, M. A. Korotin, M. Zölfl, T. Pruschke, K. Le Hur, and T. M. Rice, Electronic structure of the

heavy fermion metal LiV$_2$O$_4$, Phys. Rev. Lett. **83,** 364 (1999).

[39] S. Burdin, D. R. Grempel, and A. Georges, Heavy-fermion and spin-liquid behavior in a Kondo lattice with magnetic frustration, Phys. Rev. B **66,** 045111 (2002).

[40] J. Hopkinson and P. Coleman, LiV$_2$O$_4$: Frustration induced heavy fermion metal, Phys. Rev. Lett. **89,** 267201 (2002).

[41] S. Doniach, The Kondo lattice and weak antiferromagnetism, Physica (Amsterdam) **91B+C,** 231 (1977).

[42] S. Yamashita, T. Yamamoto, Y. Nakazawa, M. Tamura, and R. Kato, Gapless spin liquid of an organic triangular compound evidenced by thermodynamic measurements, Nat. Commun. **2,** 275 (2011).

[43] Supplemental Material at http://link.aps.org/supplemental/10.1103/PhysRevLett.132.226503 for experimental details, which includes Refs. [44,55,56].

[44] L. T. Nguyen, T. Halloran, W. Xie, T. Kong, C. L. Broholm, and R. J. Cava, Geometrically frustrated trimer-based Mott insulator, Phys. Rev. Mater. **2,** 054414 (2018).

[45] G. Cao and L. E. De Long, *Physics of Spin-Orbit-Coupled Oxides* (Oxford University Press, New York, 2021).

[46] L. E. Delong, G. W. Crabtree, L. N. Hall, H. Kierstead, H. Aoki, S. K. Dhar, K. A Gschneidner, Jr., and A. Junod, Normal and superconducting state properties of U$_6$Fe at low temperatures and high magnetic fields, Physica (Amsterdam) **135B,** 81 (1985).

[47] Yu Zhang, P. Schlottmann, R. Nandkishore, L. E. Delong, and G. Cao, Current-sensitive Hall effect in a chiral-orbital-current state, Nat. Commun. **15,** 3579 (2024).

[48] N. W. Ashcroft and N. D. Mermin, *Solid State Physics* (Holt-Saunders International Editions, New York, 1976), p. 322.

[49] N. Wakeham, A. F. Bangura, X. Xu, J.-F. Mercure, M. Greenblatt, and N. E. Hussey, Gross violation of the Wiedemann–Franz law in a quasi-one-dimensional conductor, Nat. Commun. **2,** 396 (2011).

[50] H.-Y. Xie and M. S. Foster, Transport coefficients of graphene: Interplay of impurity scattering, Coulomb interaction, and optical phonons, Phys. Rev. B **93,** 195103 (2016).

[51] Shuaishuai Luo, Feng Du, Dajun Su, Yongjun Zhang, Jiawen Zhang, Jiacheng Xu, Yuxin Chen, Chao Cao, Michael Smidman, Frank Steglich, and Huiqiu Yuan, Direction-dependent switching of carrier type enabled by Fermi surface geometry, Phys. Rev. B **108,** 195146 (2023).

[52] C. Castellani, C. DiCastro, G. Kotliar, P. A. Lee, and G. Strinati, Thermal conductivity in disordered interacting-electron systems, Phys. Rev. Lett. **59,** 477 (1987).

[53] C. L. Kane and M. P. A Fisher, Thermal transport in a Luttinger liquid, Phys. Rev. Lett. **76,** 3192 (1996).

[54] D. B. Karki, Wiedemann-Franz law in scattering theory revisited, Phys. Rev. B **102,** 115423 (2020).

[55] S. Luo *et al.*, Direction-dependent switching of carrier type enabled by Fermi surface geometry, Phys. Rev. B **108,** 195146 (2023).

[56] L. E. De Long, Phenomenological Trends for Heavy Fermi Liquids and Narrow-Band Metals, Phys. Rev. B **33,** 3556(R) (1986).